Published in final edited form as:
Auton Neurosci. 2013 October ; 177(2): 129–142. doi:10.1016/j.autneu.2013.03.008.

Vagal Afferent Innervation of the Lower Esophageal Sphincter

Terry L. Powley*, **Elizabeth A. Baronowsky**, **Jared M. Gilbert**, **Cherie N. Hudson**, **Felecia N. Martin**, **Jacqueline K. Mason**, **Jennifer L. McAdams**, and **Robert J. Phillips**
Purdue University, Department of Psychological Sciences, West Lafayette, IN 47907-2081

Abstract

To supply a fuller morphological characterization of the vagal afferents innervating the lower esophageal sphincter (LES), specifically to label vagal terminals in the tissues forming the LES in the gastroesophageal junction, the present experiment employed injections of dextran biotin into the nodose ganglia of rats. Four types of vagal afferents innervated the LES. Clasp and sling muscle fibers were directly and prominently innervated by intramuscular arrays (IMAs). Individual IMA terminals subtended about 16° of arc of the esophageal circumference, and, collectively, the terminal fields were distributed within the muscle ring to establish a 360° annulus of mechanoreceptors in the sphincter wall. 3D morphometry of the terminals established that, compared to sling muscle IMAs, clasp muscle IMAs had more extensive arbors and larger receptive fields. In addition, at the cardia, local myenteric ganglia between smooth muscle sheets and striated muscle bundles were innervated by intraganglionic laminar endings (IGLEs), in a pattern similar to the innervation of the myenteric plexus throughout the stomach and esophagus. Finally, as previously described, the principle bundle of sling muscle fibers that links LES sphincter tissue to the antropyloric region of the lesser curvature was innervated by exceptionally long IMAs as well as by unique web ending specializations at the distal attachment of the bundle. Overall, the specialized varieties of densely distributed vagal afferents innervating the LES underscore the conclusion that these sensory projections are critically involved in generating LES reflexes and may be promising targets for managing esophageal dysfunctions.

Keywords

antrum; cardia; GERD; lesser curvature; mechanoreceptor; nodose ganglion; pylorus; visceral afferent

Introduction

The need for a detailed understanding of the innervation of the lower esophageal sphincter (LES) is emphasized by the facts that the sphincter maintains fundamental esophageal and gastric functions (e.g., Boeckxstaens, 2005; Hershcovici et al., 2011; Mittal, 2012) and that dysfunctions of the LES are implicated in major esophageal disorders including gastroesophageal reflux disease (GERD), Barrett's esophagus, achalasia, Chagas disease, etc. (e.g., Giuli et al., 1998; Falk, 2002; Anand and Katz, 2010; Grassi, et al. 2011). This need for information about the innervation of the LES has been acknowledged repeatedly

*Corresponding Author: Terry L. Powley, Purdue University, Department of Psychological Sciences, 703 Third Street, West Lafayette, IN 47907-2081, Telephone: 765-494-6269, Fax: 765-496-1264 powleytl@psych.purdue.edu.

(e.g., Mittal et al., 1995; Goyal et al., 2001; Vandenplas and Hassall, 2002; Kessing et al., 2011). However, the recognition of the lack of information notwithstanding, only limited structural data are yet available. Further, those descriptions that are available are focused largely on the efferent projections.

For the most part, the afferent innervation of the sphincter has been explored only incidentally in the course of general surveys of the lesser curvature. Early neural tracing experiments did establish that the LES receives vagal afferent innervation (Mei et al., 1972; Falempin et al., 1978; Clerc and Condamin, 1987; Mazzia and Clerc, 1997), but they provided little information on the precise distributions and morphology of the terminals. In addition, later broad surveys of the vagal afferent innervation of the esophagus and stomach with tracers have observed that *intraganglionic laminar endings* (IGLEs) and *intramuscular arrays* (IMAs), the two basic types of mechanoreceptors found throughout most of the stomach, also occur in the region of the LES (rats: Neuhuber et al., 1998; Wang and Powley, 2000; mice: Fox et al., 2000). Additionally, a recent inventory of vagal afferents innervating the gastric antrum characterized exceptionally long IMAs innervating the conspicuous principle sling muscle bundles or bands that course between the muscular ring of the LES and the antropyloric region (Powley et al., 2012). Furthermore, the same experiment reported that the distal attachment of this principle sling muscle bundle is also innervated by a specialized net-shaped afferent terminal, a *vagal web afferent,* that has a restricted distribution at a site near where the sling bundle attaches.

Still, neither the earlier tracer surveys nor the recent inventory of antral afferents focused specifically on those afferents that project to the clasp or the sling muscle fibers that encircle the gastroesophageal junction and form the functional lower esophageal sphincter. To extend understanding of the sensory mechanisms of the LES, the present experiment sought to inventory, and then to better characterize, the vagal afferent innervation supplied to the collar-shaped muscular wall of the LES comprised of clasp and sling muscle fibers.

Materials and Methods

Animals

Male Sprague-Dawley rats (n = 40; Harlan, Indianapolis, IN, USA) weighing 237 ± 6.4 gm at the time of tracer injection were housed individually in an AALAC-approved colony room maintained at 22–24 °C on a 12:12 hour light:dark schedule. The animals were provided with chow (Laboratory diet no. 5001; PMI Feeds, Inc., Brentwood, MO, USA) and tap water available ad libitum, except for the night prior to surgery. All procedures followed the guidelines of *The NIH Guide for the Care and Use of Laboratory Animals* (8^{th} ed., The National Academic Press, Washington, D.C.), and were approved by the Purdue University Animal Care and Use Committee. Throughout the experiment, every effort was made to minimize suffering and the number of animals used. To this end of minimizing animal number and suffering, we also augmented the sample of afferents in the present survey by scanning and sampling (see below) similarly prepared tissue specimens from an earlier experiment (Powley et al., 2012).

Neural Tracer Labeling

Animals were anesthetized with Isoflurane (Isoflo®; Abbott Laboratories, North Chicago, IL, USA) and injected with Glycopyrrolate (0.2 mg mL^{-1}, s.c.; AmericanRegent Inc., Shirley, NY, USA), following an overnight fast. The left and right nodose ganglia were exposed through a midline incision of the skin of the ventral neck and by subsequent blunt dissection of the overlying muscles.

The ganglia were injected bilaterally, using a protocol that yields, with each individual injection, complete labeling of a random fraction of all nodose neurons. Much like the Golgi technique, this limited labeling strategy makes it practical to examine and digitize individual neurites and their terminals without the ambiguities that occur with excessively dense and tangled fields of stained neural processes. Specifically, 1 μL of a dextran solution consisting of a 1:1 mixture of 3K and 10K MW lysine-fixable dextran biotin (final concentration: 15%; consisting of 7.5% D7135 and 7.5% D1956, respectively; Invitrogen, Carlsbad, CA, USA) was injected into each ganglion. The tracer solution contained 0.01 mg of Fast Green FCF (Sigma-Aldrich, CO, USA) per 100 μL to facilitate visually monitoring the distribution of injected tracer solutions within the nodose. The skin was then closed with interrupted sutures, and the rats were recovered on a circulating-water warming pad prior to being returned to their home cages, where they were again provided with ad libitum food and water. The animals received 0.01 mg kg^{-1} of Buprenorphine subcutaneously (Buprenex®, Reckitt Benckiser Pharmaceuticals Inc., Richmond, VA, USA) prior to closure of the incision and then again the next morning.

Tissue Fixation and Dissection

Fourteen days post-injection, rats were given a lethal dose of sodium pentobarbital (180 mg kg^{-1}, i.p.) and, when completely unresponsive, transcardially perfused with physiological saline followed by 4% paraformaldehyde in 0.1 mol L^{-1} phosphate-buffered saline (PBS, pH 7.4). To fix the stomachs in a state of normal distension and accommodation, the animals had access to food until the time they were over-anesthetized for perfusion, and then, during the vascular saline perfusion for exsanguination, 10 ml of physiological saline at body temperature was concurrently infused slowly by catheter into the stomach.

After perfusion, the stomachs were removed en bloc and trimmed to yield whole mounts that contained the LES, the antral wall, and the pylorus (see Fig. 1). Specifically, the stomach was separated from the duodenal bulb at a point preserving the pylorus with the gastric whole mount (Fig 1A and 1B). Next, an incision was made along the full length of the greater curvature from pylorus to the transition to lesser curvature in the forestomach (approximately at the fundus/corpus boundary). To reduce the gastric specimen to a pylorus-antrum-esophagus whole mount, a cut was started at the distal greater curvature near the corpus-antrum border (Fig. 1A). The cut was then extended rostrally with an arcing incision that roughly paralleled the greater curvature before wrapping medially to the angle of His. On the opposite wall of the stomach, the cut then continued paralleling the greater curvature in a line that traversed the corpus and antrum to return to the distal greater curvature.

Once the specimen had been trimmed to size, a slit in the ventral (or occasionally dorsal) gastric wall was made to reduce cupping of the cardia and to flatten the whole mount. The cut spanned from the edge of the whole mount to the lumen of the esophagus. Using the schematic in Figure 1C as reference, this incision to reduce cupping was made between 2:00 and 4:30 (or, in the case of dorsal cuts, 7:30 and 10:00). These locations for the incisions, roughly along a left-right equatorial line that intersected the center of the esophageal lumen, were chosen because (a) for the planned morphometry and analysis of the terminals (see below and see Results), we anticipated not classifying terminals along the equator since clasp and sling muscle fibers interdigitate extensively in those regions and distinguishing muscle types associated with the IMAs in the regions was too problematic, and (b) the incisions in the whole mounts typically damaged the afferent terminals in the immediate region. Once the whole mount was isolated and incised, the mucosa and submucosa were removed by dissection.

Staining

Whole mounts were processed as free-floating specimens. The tissue was treated with a hydrogen peroxide:methanol block (1:4) to quench endogenous peroxidase activity, soaked for 3–5 days in PBST (PBS containing 0.5% Triton X-100 and 0.08% Na azide) to facilitate penetration. Specimens were then incubated for 1 h in avidin-biotin-horseradish peroxidase complex (PK-6100; Vectastain Elite ABC Kit, Standard; Vector Laboratories Inc., Burlingame, CA, USA). The tissue was next rinsed in PBS and reacted with diaminobenzidine (DAB) and H_2O_2 for 5 min to yield a permanent golden-brown stain of labeled neurites.

In order to optimize both the visibility and clarity of the tracer staining in the thick specimens of muscle wall, the whole mounts were not counterstained. Once processed with DAB, the whole mounts were simply rinsed and mounted serosa-side-up on gelatin-coated slides. The specimen was then air dried, dehydrated in alcohol, cleared in xylene, and coverslipped with D.P.X. (317616; Sigma-Aldrich, St. Louis, MO, USA).

Afferent Terminal Assessments, Image Analysis, and Photography

Analysis of the labeled vagal afferent projections was done in stages. Whole mounts were first scanned in their entirety, using brightfield and differential interference contrast (DIC) optics on Leica DMRE and DM5500 microscopes equipped with long working distance objectives. Tracer-labeled neurites and terminals were inventoried as to location.

Once all the labeled fibers had been identified, their terminal specializations were categorized. The fibers and endings were then assessed for the density of the tracer labeling, apparent completeness (free of tears, damage, etc.) of the neurite, and adequacy of exposure for imaging (not obscured by folds or other tissue artifacts, etc). Out of the complete inventory produced in the initial scans, the afferent terminals most adequately satisfying the criteria for complete analysis were then mapped onto a normalized schematic of the LES, antrum, and pylorus (cf. Fig. 1C). For reference, small subsets of well labeled antral, pyloric, and web ending fibers, as shown on the schematic, were also examined.

Finally, since our initial survey indicated that vagal intramuscular arrays (IMAs) comprise the basic innervation of the muscle wall of the LES (see Results), those clasp and sling muscle IMAs that best satisfied the staining criteria just mentioned, were digitized, reconstructed, and evaluated quantitatively on a Neurolucida (MircoBrightField Inc., Williston, VT, USA) workstation employing a Zeiss Axio Imager Z2 microscope equipped with DIC optics and long working distance objectives.

For the Neurolucida tracing and quantitative analysis, an additional criterion was used to distinguish clasp from sling muscles with their respective IMAs: Clasp muscle fibers are organized as a “U”-shaped yoke that loops around the distal or antral pole of the esophageal wall, whereas sling fibers form an inverted “U”-shaped yoke that loops around the rostral or forestomach pole of the esophageal wall towards the angle of His. At the ventral and dorsal gastric wall sides of the gastroesophageal junction the smooth muscle fibers of the two yokes —in effect the arms of the two yokes--intermingle most extensively. For the full quantitative characterizations of terminals, we avoided including IMAs located in this region where the intermingling occurs. As illustrated in the schematic whole mount in Figure 1C, we established a horizontal equatorial line that extended from left to right, intersecting a point in the middle of the esophageal lumen. Then to distinguish clasp from sling afferent endings, terminals that fell within ±15° of the equatorial line were excluded to avoid mistaken identifications in the region where the muscle fibers interdigitate. (As described above, the incisions made in the whole mounts to minimize the cupping of the cardia also were made close to the equatorial line, often damaging afferent terminals in the immediate

area.) For the 3D morphometric reconstructions and quantitative analyses, vagal afferent terminals within a 9 mm radius of the esophagus (see above) and distal to this ±15° zone of intermingling were classified as *clasp muscle endings*, whereas terminals within the 9 mm radius and rostral to the ±15° zone were considered *sling muscle endings*.

Single field photomicrographs were acquired digitally with a Spot Flex camera controlled using Spot Software (V4.7 Advanced Plus; Diagnostic Instruments, Sterling Heights, MI, USA). To maximize the depth of field of some images, Helicon Focus Pro X64 software (V5.3.7; HeliconSoft Ltd., Kharkov, Ukraine) was used to merge z-stacks of images taken at different z-planes (i.e., focus stacking).

For images of more extensive terminal arbors, mosaics or multiple-field composites of high magnification images were prepared using Surveyor with Turboscan software (V. 6.0.5.3; Objective Imaging, Cambridge, UK) on a Leica DM5500 workstation. Z-stacks of mosaic images of the IMA arbors were also generated, exported to Photoshop CS5 (Adobe Systems, San Jose, CA, USA), and then used to trace arbors. In contrast to Neurolucida tracings, which yield formalized stick-figure facsimiles of arbors (e.g., Fig. 5 below), Photoshop tracings that created 2D planar projection images from 3D stacks of photomicrographs readily included more complete features (dilations, lamellae, etc.) and more realistic caliber-accurate neurites (e.g., Figs. 3 and 4 below) than Neurolucida.

For figure production, Photoshop CS5 was also used to (1) apply text and scale bars, (2) adjust brightness, contrast, and sharpness, and (3) organize the final layouts of the figures.

Statistics

Statistical comparisons consisting of unpaired t-tests were generated using GraphPad Prism (V. 5.0; GraphPad Software, San Diego, CA, USA).

Results

The whole mount protocol yielded specimens with high definition staining of tracer-labeled neurites, making it practical to survey the thick muscle wall forming the LES (Fig. 1; also see Fig. 6 below for an illustration of a terminal, an IGLE, located between unstained muscle layers). Four basic vagal afferent specializations consistently occurred in conjunction with the LES, and virtually all of the sample of LES-associated afferents that were inventoried consisted of variants of one of the four types of endings. Two of the four were found within the sphincter: These types were (1) IMAs innervating the clasp and sling muscle fibers of the sphincter ring, (2) IGLEs innervating the myenteric plexus between muscle sheets of the sphincter. The other two types of afferents were associated with the principle bundle of sling muscle fibers that spanned between the sphincter ring and the distal antropyloric lesser curvature: These associated types were (3) the highly elongated and specialized IMAs found exclusively in the principle bundle of sling muscle fibers, and (4) the unique antral web afferents, which we recently described (Powley et al, 2012), that innervate the distal antral site of attachment of the principle bundle of sling muscle fibers.

Out of the inventory (> 250 endings) from the first-stage survey, those afferent terminals most adequately satisfying the criteria for complete analysis were then mapped onto a normalized topographic schematic of the LES, cardia, antrum and pylorus (cf. Fig. 1C) and digitized and evaluated with the Neurolucida tracing software. (For reference, smaller subsets of antral and pyloric fibers were also examined, and they are also shown on the schematic.)

IMAs innervate LES smooth muscle fibers

Intramuscular arrays were the only vagal afferents that directly innervated the smooth muscle fibers of the LES, and they had a particularly prominent and extensive distribution in the clasp and sling fiber bundles that comprise the LES. The basic architecture and planar organization of an IMA is illustrated with a Neurolucida stick figure in Figure 2. Like IMAs observed in other regions of the stomach, they were highly elongated (1.5–2.5 mm “long”--see Fig 2), planar (20–30 μm deep or “thick”--Fig. 2C) arbors of terminal neurites (150–250 μm “wide”--Fig 2A). In the initial inventory of endings, IMAs were found arrayed around the entire sphincter so as to create a complete 360° annulus of arbors within the sphincter muscle. IMAs appeared equally densely distributed around the sphincter ring, though the clasp and sling IMAs that were sampled for the quantitative morphometry were taken from the “poles” of the sphincter along a mid-sagittal line, where the ambiguities of muscle type and problems of incision damage were minimal.

IMAs innervated the muscle fibers in the *clasp muscle* bundles, i.e. those bundles that arch through the lesser curvature at the esophagogastric junction, forming in effect the antral and distal wall of the esophageal sphincter (see Fig. 3 and Fig. 5). These IMAs exhibited the conventional defining features found in IMAs throughout the stomach. In particular, the clasp IMAs ramified into terminal arrays of long neurites running both parallel to and in tight approximation to the smooth muscle fibers that formed the clasp bundles. These neurites were interconnected by shorter bridging elements that spanned from one muscle fiber over to a neighboring muscle fascicle to elaborate another neurite associated with that fascicle. Along their trajectories, the neurites variously displayed both smooth and lamellar segments. In keeping with the orientations of these circular and oblique fibers, the neurites of the clasp IMAs tended to describe gradual arcs that paralleled the circumference of the esophagus.

In the *sling muscle* fiber bundles that arch around the forestomach side of the LES to form its angle of His or greater curvature wall, the muscle fibers were again innervated by IMAs similar in appearance to those that innervated the clasp muscles (see Fig. 4; also see Fig. 5). The sling muscle IMAs, like other gastric IMAs were also comprised of long parallel neurites, in apparent contact with the muscle fibers and interconnected by shorter bridging elements. Like the IMAs in clasp muscle bundles, those IMAs in sling muscle also were oriented as arrays of concentric arcing neurites that paralleled the circumference of the esophagus. In another similarity to the organization of the afferents in the clasp bundles, the IMAs constituted the only type of vagal afferent fiber in the sling bundles.

Two additional features of the IMA architecture in the LES were noteworthy. First, though the majority of both clasp and sling muscle IMAs conformed simply to the general patterns just described (see also Figure 5), a small minority of the IMAs associated with the smooth muscles forming the LES had, in addition to the same defining arbors of neurites paralleling smooth muscle fibers, a collateral branch that ended as a dense calyx or basket of terminal plates or varicosities that appeared to be encapsulating an unstained tissue element. Second, a substantial part of the terminal neurites forming the IMAs often had lamelliform or growth-cone-like profiles.

Given the prominence of IMAs in the sphincter region, given the fact that the IMAs directly innervate the sphincter smooth muscle, and given the lack of previous observations on these afferents, a quantitative morphometric assessment of this type of LES afferent was performed.

Statistical Comparisons of Clasp and Sling Muscle IMA Arbors

A quantitative comparison of the IMAs innervating clasp muscles versus those innervating sling muscles highlighted significant differences consistent with local muscular specializations. Clasp muscle IMAs (n = 63; see Fig. 1C) were significantly larger and more extensive than sling muscle IMAs (n = 32; Fig. 1C). Specifically, individual clasp IMAs innervated twice the area occupied by sling IMAs (434,064 μm^2 vs. 214,880 μm^2, p = 0.001). This increase in innervated area or "receptive field" was generated by a greater complexity on several dimensions. Clasp endings had significantly longer arbors than sling IMAs (the length of the arbor or "Y" dimension was the axis that paralleled the smooth muscle fibers and the circumference of the esophagus: clasp = 2274 ± 185 μm vs. sling = 1609 ± 185 μm; p = 0.02). Clasp IMAs also elaborated significantly more branches than sling IMAs: in particular, clasp IMAs branched significantly more times (82.14 ± 5.87 vs. 43.47 ± 4.91, p = 0.0001), clasp IMAs had significantly greater highest order branches (16.52 ± 0.67 vs. 14.13 ± 0.79, p = 0.03), and clasp IMAs had significantly more total branches (165.3 ± 11.74 vs. 87.91 ± 9.82, p = 0.0001). Overall, the aggregate of greater branch complexity of the clasp IMAs compared to the sling IMAs on several dimensions generated a nearly two-to-one greater sum total length of neurite branches per arbor (11,112 ± 830 μm vs. 6,244 ± 762 μm, p = 0.0002).

The pattern of clasp endings having longer and more extensive receptive fields can be seen by comparing the clasp IMA tracing in Figure 3 with the sling IMA tracing in Figure 4. Similarly, Figure 5 contains a sample of representative IMA tracings, and the same pattern of clasp endings being somewhat longer and more extensive can be seen there as well.

Interestingly, while the clasp IMAs were larger and more extensive than the sling IMAs, not all arbor parameters were greater. Neither the width of the clasp IMA arbors ("width" or X-value was measured on a vector parallel to the muscle wall sheets and orthogonal to the long axis of smooth muscle fibers: clasps: 197.8 ± 17.6 μm vs. slings: 158.7 ± 27.8 μm, p = 0.22, n.s.) nor the "thickness" of the clasp IMA arbors ("thickness" or "depth" or Z-value was measured on a vector perpendicular to the muscle sheets: clasps: 24.02 ± 2.11 μm vs. slings: 25.41 ± 3.82 μm, p = 0.73, n.s.) differed from those of the sling IMA arbors. In addition, another dimension on which the clasp and the sling IMAs did not differ--and which may be particularly instructive in terms of how IMA architecture is formed--was average branch length: Though the clasp IMAs branched more extensively and formed more branches than the sling IMAs (above), the two types of IMAs did not differ in the mean length of the individual branches in their arbors (clasp: 69.63 ± 3.71 μm vs. sling: 82.13 ± 9.77 μm, p = 0.16, n.s.).

The IMAs in the LES region were located deep in the muscle wall, immediately superficial to the boundary between the muscularis and the submucosa, as was previously noted by Neuhuber and colleagues in their early survey of esophageal afferents (1998). To gauge this location in our samples, we measured the depth, or location on a serosa-to-submucosa axis (or "Z-axis") of those clasp muscle IMAs and sling muscle IMAs that had no interfering processing artifacts (n = 56 and n = 29, respectively). In the flattened whole mounts, the muscle wall varied significantly (p = 0.05) in thickness, with the clasp muscle tissue in the lesser curvature being thicker than the sling muscle wall in the angle of His (88.46 ± 4.76 μm vs. 73.79 ± 4.80 μm, respectively). For comparison, the IMAs, which did not differ in the Z-dimension or "thickness" of their arbors (~ 24.5 μm), spanned roughly a third of this serosa-to-submucosa distance. Both clasp and sling IMAs were located at the submucosal boundary. The two groups (i.e. clasp and sling) of IMAs had essentially identical (p = 0.24, n.s.) distances between the deepest neurite of each of the individual arrays and the muscle-submucosal boundary (clasp IMAs = 3.04 ± 0.77 μm; sling IMAs = 4.90 ± 1.60 μm). Because the clasp vs. sling muscle walls varied in thickness while the two types of IMAs did

not differ in thickness, the comparably deep locations of the clasp and sling IMAs meant that the two types of IMAs were significantly ($p = 0.02$) different distances (61.41 ± 4.7 μm vs. 43.48 μm, respectively) from the more superficial serosal-muscularis boundary.

Finally, the analyses of the clasp and sling IMAs generated another instructive measure that elaborates on the observation that these vagal afferents are organized to encircle or create a mechanoreceptor annulus around the LES. Using (a) the distance of the individual IMAs from a center point in the esophageal lumen to the midpoint of the IMA terminal arbor as well as (b) the full length of the arbor, which was oriented parallel to the associated smooth muscle fibers that encircled the esophagus, we calculated the angle or degrees of arc of the LES ring that individual IMAs subtended. Clasp IMAs subtended an average of 19.7±3.3 degrees of LES arc per IMA, whereas sling IMAs individually subtended an average of 13.5±1.9 degrees of LES arc. This trend for clasp IMA arbors to have somewhat greater degrees of arc is consistent with the clasp endings having larger and more extensive receptive fields than sling IMAs, but the trend for degrees of arc was not significant ($p = 0.08$). Combined to generate a global overall mean, since the trend was not significant, the pooled clasp and sling IMAs spanned individually--presumably transduced--an average of 15.7±1.7 degrees of LES circumference.

IGLEs innervate myenteric ganglia throughout LES region

As predicted from the limited earlier morphological observations (Berthoud et al., 1997; Neuhuber et al., 1998; Wang and Powley, 2000) and electrophysiological reports suggesting vagal afferents sensitive to tension are located near or in the LES (Mei et al., 1972; Falempin et al., 1978; Clerc and Mei, 1983; Zagorodnyuk and Brookes, 2000), the myenteric ganglia between smooth muscle layers were innervated by IGLEs. Notably, IGLEs were observed on myenteric ganglia between the smooth muscle layers in the cardia (see Fig. 6, right column) as well as on those ganglia associated with bundles of esophageal striated muscle that extended as far distal as the region of the LES (see Fig. 6, left column). In contrast to IMAs, which seemed to be adapted to the particular characteristics of the clasp and sling muscle collar around the LES, IGLEs in the region of the cardia did not have an obvious specialization in either structure or distribution.

LES is also innervated by two vagal afferent specializations associated with principle bundle of sling muscle

In addition, the present series of LES-plus-antrum whole mounts included the elongated strap-like principle bands of distal sling muscle that lie relatively superficial in the rat lesser curvature and are anchored distally in the region of the pyloric antrum (illustrated in the schematic in Figure 1C). Correspondingly, the present series of whole mounts also included the exceptionally elongated IMAs (8 millimeters, in contrast to the 1–2.5 millimeters of the IMAs just described in the clasp and sling muscle bands encircling the esophagus to form the LES) that innervate the conspicuous bundles (Fig 7).

Finally, the apparently unique vagal afferent specialization that was recently described and designated an *antral web ending* and found apparently only in the region where the sling muscle bands anchor distally in the antrum-pylorus junction (Powley et al., 2012) also occurred in the present tissue samples (Fig. 8). As previously reported, the web endings were essentially planar plate-like subserosal structures located parallel to and superficial to the antral muscle layers. These endings were readily distinguished from both IGLEs and IMAs not only by their location, but also by their distinctive “net” or honeycombed web arbors comprised of highly lamelliform terminal elements (compare, for example, the web ending in Fig. 8 with the IGLEs in Fig. 6 and the IMAs in Figs. 3 and 4).

Both the conspicuously elongated IMAs innervating the principle sling muscle bundles and the unusual arbors of the web endings provided useful contrast with the clasp and sling muscle IMAs insofar as neither antral fiber specialization was found in the ring of muscle bundles constituting the LES proper.

Discussion

A detailed understanding of the innervation of the LES--particularly its afferent innervation--has not been available. To begin to redress the lack of information, the present survey delineates the terminal morphology and distribution of the vagal afferent innervation of the region. The survey indicates that the vagus supplies four different afferent specializations to the LES and its attachments to the antral wall, with the vagal intramuscular arrays (IMAs) in both the clasp and sling musculature of the sphincter constituting prominent--and the only--vagal afferent endings associated with the sphincter muscle fibers per se. These IMAs, putative stretch receptors, are distributed within the sheets of clasp and sling muscle fibers so as to create an annulus of concentrically distributed mechanoreceptors that completely encircle the gastroesophageal junction.

The present results can be considered in terms of these IMAs and the other specialized afferent terminals that innervate the muscle wall of the LES, notably the intraganglionic laminar endings (IGLEs) located between the muscle sheets and innervating the local myenteric plexus, and then in terms of some of the functional and therapeutic implications of these specializations. First, though, a consideration of the limits of the present inventory offers perspective.

Adequacy and Limitations of the Present Inventory of Vagal Afferents Innervating the LES

Significant impediments to surveying the LES musculature for its innervation are the three-dimensional complexity of the structure and the heavy muscle bundles that form this “functional” sphincter. The spatial extent and the complexity of the region create imposing difficulties for attempts to examine the region with conventional tissue sectioning technologies. Whole mount protocols can circumvent some of those difficulties, but the tissue thickness of the region commonly compromises whole mount preparations as well. Impediments that complicate preparing the LES and antrum as whole mounts include the excessive tissue thickness that can (a) limit the penetration of stains and labeling antibodies, (b) obscure or mask detail when counterstains are employed, and (c) exceed the working distance of microscope objectives.

In a recent survey of the antrum (Powley et al., 2012), we adapted whole mount preparation procedures and neural tracer techniques for the particularly thick lesser curvature and found that the adaptations effectively minimized the difficulties of imaging labeled afferents in whole mounts of the thick tissue. The trimming of the tissue and the removal of the mucosa and submucosa produced a specimen that could be flattened and examined. Eliminating routine counterstaining, which tends to darken and cloud thick specimens, and relying on differential interference contrast optics to observe tissue elements provided good —even Golgi quality--contrast. Furthermore, we could regularly follow individual fibers and evaluate their complex terminal elements throughout the whole mount specimens, indicating that the use of biotinylated dextran as a tracer combined with avidin and DAB processing avoided problems of solutions penetrating the tissues.

Given the quality of the labeling and the size of the sample surveyed, it is likely that the four types of afferents we observed in the present experiment represent a comprehensive set of the classes of sensory terminals the vagus nerve supplies to the muscle wall of the LES region and the principle bundle of sling muscle that connects the LES and antrum. Both the

size of the pool of animals (n = 40) and the number of individual fibers identified and evaluated (n > 250) were large enough that we should have sampled any common types of vagal afferent projections to the region.

Intramuscular Arrays (IMAs) Innervate Clasp and Sling Muscle Fibers

IMAs were found intercalated within the fascicles of both clasp and sling muscle fibers that encircle the gastroesophogeal region designated the LES. These IMAs were arrayed parallel to the circumference of the wall of the esophagus. Generally, then, the IMAs of the LES establish a band or collar of concentrically arrayed sensors disposed to transduce distortions of the clasp and sling muscle fibers. Individual IMA arbors subtended roughly 16° of esophageal arc. Collectively, these separate IMAs of the clasp and sling muscle bundles comprised a 360° ring or annulus of mechanoreceptors in the muscle wall of the LES.

Given their structure and given that they are intercalated among muscle fibers, IMAs are considered mechanoreceptors. Even more particularly, IMA terminal arbors have structural features, regional distributions, and articulations with interstitial cells of Cajal and muscle fibers (Phillips and Powley, 2000; Powley et al., 2008; Powley and Phillips, 2011) that suggest that the afferents operate as stretch receptors. As stretch or length detectors concentrically encircling the gastroesophageal junction, the afferents would presumably report whether the LES was closed or in a state of partial to complete opening.

A limited number of electrophysiological experiments have recorded from morphologically unspecified vagal afferents with receptive fields in the region of the LES (Mei et al., 1972; Falempin et al., 1978; Clerc and Mei, 1983; Clerc, 1984). Such experiments commonly distended the tissues of the LES by inflating or mechanically stretching the sphincter region. These physiological experiments reinforce the conclusion that vagal afferents innervating the region operate as mechanoreceptors. The initial electrophysiological observations have most frequently been discussed primarily in terms of tension receptor responses, however conventional distension paradigms do not distinguish between tension and stretch. Forces of tension and stretch are typically confounded when a viscus is inflated or distended. More specific experiments that independently manipulate stretch under isotonic conditions and that vary tone under isometric conditions and that simultaneously determine whether the afferent terminal being monitored is an IMA or another species of mechanoreceptor will be needed to ultimately determine the type of mechanical forces the annulus of IMAs is transducing. Meanwhile, however, it seems clear from the prominent ring of IMAs that encircles the LES that the closure and opening of the sphincter is carefully monitored by these specialized vagal afferents as well as by IGLEs.

For transducing stimuli, the deep location of the clasp and sling IMAs, virtually at the submucosal boundary of the muscle wall, would presumably make the endings exquisitely sensitive to the mechanical forces within the sphincter. Stretch or other signals originating in the lumen would not be distributed or dissipated widely through the thickness of the muscularis before being transduced, but instead would be applied focally, and with short latency, to the proximately located IMAs in the LES.

Independent of the type of mechanical stimulus to which IMAs may be tuned, the present quantitative assessment of the clasp muscle IMAs versus the sling muscle IMAs is consistent with another functional inference. While clasp and sling muscle IMAs were generally similar in appearance and defining features (compare, for example, the clasp IMA in Fig. 3 with the sling IMA in Fig. 4), the quantitative analysis of the arbors revealed statistically reliable differences in a number of features including length, branching complexity, area of receptive field, etc. (see Fig. 5 also). Particularly relevant to this discovery is the fact that clasp and sling muscle fibers have been shown to have several

conspicuously different physiological properties (Brasseur et al., 2007; Mittal, 2012). Conceivably, the quantitative differences in clasp and sling IMAs might either reflect or, perhaps, contribute to such differences in clasp and sling muscle physiology. Similarly, since clasp IMAs are in the thicker-walled lesser curvature side of the gastroesophageal junction, whereas sling IMAs are in the thinner-walled angle of His and greater curvature side, the discrepancies in IMAs could reflect differences in mass of the innervated muscle bundles.

Intraganglionic Laminar Endings (IGLEs) also innervate the LES

Topographic surveys of the IGLEs in the stomach (Berthoud et al., 1997; Wang and Powley, 2000) and esophagus (Neuhuber et al., 1998, 2006) have also described IGLEs occurring in the general region of the LES. In agreement with these earlier surveys, the present inventories consistently documented IGLEs between the muscle layers where the myenteric plexus neurons (unstained in our case) are situated. Notably, as illustrated in Fig.6, because the rat has a completely striated muscle esophagus, the esophageal striated muscle bundles and gastric smooth muscle bundles interdigitated at the level of the LES, and we observed IGLEs both between layers of esophageal striated muscle (Fig. 6, left column) and gastric smooth muscle (Fig. 6, right column).

The fact that IGLEs were found between the LES muscle sheets which also contained the sphincteric ring of IMAs underscores the earlier point that it is difficult to correlate prior electrophysiological experiments on the vagal innervation of the LES with any defining regional distributional patterns. It is instructive that, in other areas of the stomach and esophagus where distributions of IGLEs are less co-extensive with major fields of IMAs, and where it has proved practical to anterogradely label individual terminals that have been characterized electrophysiologically, Zagorodnyuk and colleagues (Zagordnyuk and Brookes, 2000; Zagordnyuk et al., 2001, 2003) have demonstrated, using an organ bath preparation permitting better stimulus control, that vagal IGLEs in the neighboring sites operate as tension receptors. Such observations would suggest that potentially at least some of the vagal afferents innervating the LES that respond to distension and operate like tension receptors are the IGLEs located between those muscle sheets in the LES area.

Such an inference would also be consistent with the previously suggested hypothesis that IMAs may function more specifically as stretch receptors whereas IGLEs may indeed function as tension receptors (Phillips & Powley, 2000; Powley and Phillips, 2011). By extension, the conclusion would suggest the LES is innervated by both vagal stretch and vagal tension receptors. This hypothesized architecture would appear to be well suited to generating fine control of crucial sphincter operations. If the annulus of IMAs transduce stretch, as an index of the sphincter circumference (or diameter), and the IGLEs in the tissues of the cardia transduce tension, as an index of the distending forces that must be offset by muscular contraction, vagovagal reflexes controlling the sphincter would not be engaged by only a single type of information, but rather by using two independent, albeit frequently correlated, indices of sphincter status.

Vagal IMAs in Principle Bundle of the Sling Muscle

In an earlier examination of vagal afferents projecting to the antral region, we described the superficial straps of sling muscle fibers that span between the gastroesophageal junction and the region of the antropyloric junction in the rat (Powley et al., 2012; see also Fig. 1C). In that report, we identified exceptionally long IMAs innervating these principle bundles of sling fibers. These afferent terminals are considerably longer (e.g., ≥8 millimeters) than any other IMA variants we have observed, including those just described in the sphincter muscle ring, which are on the order of 1.5 to 2.5 millimeters in length. These elongated IMA

specializations in the distally directed bundles of sling muscle fibers were not the primary focus of the present survey, but, as illustrated in Fig. 7, they were also observed in the present series. Explanations of the afferent innervation of the LES will need to incorporate and account for these principle bundle IMAs as well as the clasp and sling IMAs that form the annulus of terminals immediately around the LES. As discussed in the earlier report, the organization of the long longitudinal bundles suggests the possibility that they play a role in coordinating LES operations with the activity of the antropyloric region.

Vagal Antral Web Ending Associated with the Principle Bundle of the Sling Muscle

Accounts of vagal afferents innervating the LES will also have to include and develop an understanding of a second, apparently unique, vagal terminal specialization associated with LES functions. This ending, which is organized in the form of a net or web (see Fig. 8) and lies relatively superficially on the serosal side of the muscle wall, is located exclusively at the distal antral site where the principle bundle of sling muscle attaches (cf. Fig. 1C).

This antral web afferent specialization was included in the present survey for multiple reasons. First, these afferents appeared regularly in the present whole mount sample. Second, since the afferent appears to be associated with the principle sling muscle bundle, the antral net should also be incorporated into explanations of the afferent innervations of the LES. Third, in undertaking the present inventory, an open question was whether these web-like terminals had as limited a distribution as that which we had observed in the distal antrum or whether web endings might also be found in conjunction with those sling fibers (and perhaps clasp fibers as well) forming the LES. The results answer this third question: The present survey routinely noted the antral web endings in the distal antral sites as previously described (Powley et al., 2012), but found no evidence of the web specialization associated with these clasp and sling muscle bundles that closely encircle the gastroesophageal junction and establish the LES.

Functional Implications of Vagal Afferent Specializations Innervating the LES

Traditionally, in accounts of LES function, the afferent innervation of the LES has been considered only cursorily and, perhaps correspondingly, not fully integrated into models of sphincter control. The present survey is an attempt to produce a more adequate characterization of the afferent elements contributing to sphincter function. Notably, the survey indicates IMAs are distributed through clasp and sling muscle fibers to create an annular surround, or collar, of mechanoreceptors, and IGLEs are associated with the myenteric plexus throughout the LES region, including both the smooth and striated muscle sheets. Including the two afferent specializations that are associated specifically with the principle bundle of sling muscle attached to the antral lesser curvature, our inventory indicates the vagus innervates the LES musculature with four different species of vagal afferents.

These four afferent types presumably initiate and regulate vagovagal and possibly other reflex loops that control the operation of the LES. Disordered functioning of any of the four species of afferent terminals might generate erroneous sensory signals and skew reflex adjustments orchestrated by vagal preganglionic or sympathetic postganglionic motor neurons innervating the sphincter. In such a scenario, a dysphagia or reflux disease would be the result of distorted afferent information. Presumably, in such cases of “primary afferent dysfunction,” interventions or therapies targeted to the affected afferents would be the obvious treatment. Indeed, the present results suggest that both IMAs and IGLEs offer logical targets for pharmacological therapies designed to improve sphincter function.

In this vein, it should be noted that some attention has been focused on the idea of treating vagal afferents as therapeutic targets for gastrointestinal disorders. Such an approach has been considered abstractly (e.g., Powley et al., 2005; Beyak, 2010; Hershcovici et al., 2011), and it has been employed in animal models and in limited clinical applications for LES disorders. In a particularly relevant case, in both animal models and patients with reflux disease, the triggering of transient LES relaxations by gastric distensions is inhibited with antagonists of the glutamate MGluR5 receptor (Frisby et al., 2005; Jensen et al., 2005; Lehmann, 2008; Zerbib, 2010). Significant efforts have also been directed towards characterizing the neurochemical phenotypes of vagal afferents, with a view to how they might be manipulated pharmacologically (e.g., Beyak and Grundy, 2005; Helke, 2005; Brierley et al., 2006). To date, though, most of the pharmacological interventions and phenotypic characterizations have been attempted on global or largely undifferentiated populations of “vagal afferents” or “nodose afferents” or “vagal afferents responding to stomach distension,” without reference to their particular type (IMA vs. IGLE, etc.) or location (LES vs. antrum, etc.). Such inclusive sampling makes it problematic to formulate clear predictions for the sphincteric clasp or sling muscle IMAs or for how LES IMAs could be selectively manipulated without affecting, perhaps counterproductively, the IGLEs in the same region. Recently, analyses to distinguish the phenotypes of more specific subpopulations have been undertaken (e.g., Page et al., 2005; Bielefeldt et al., 2006; Slattery et al., 2006; Page et al., 2007; Timmermans and Adriaensen, 2008), and future more selective pharmacological therapies can be anticipated.

In the event that the vagal afferents innervating the LES of an individual with a reflux disorder or dysphagia operated normally and were not disordered, an alternative therapeutic implication of the extensive afferent innervation pattern may also need to be considered. Regardless of the underlying etiology of GERD and dysphagias, those therapeutic interventions which are not simply palliative have commonly focused on the motor tone of the organ. Such pharmacological treatments designed to affect the tone or excitability of the effectors or the motor arm of the relevant reflex loops might provoke the LES afferents to initiate compensatory or counter-regulatory adjustments that would tend to cancel or minimize the impact of the therapy. If such complications should occur, the motor interventions might be made more efficacious by combining them with parallel interventions that would cancel the afferent error signals.

Acknowledgments

This work was supported by grants from the National Institutes of Health, USA (DK27627 to TLP; DK61317 to RJP and TLP).

References

Anand G, Katz PO. Gastroesophageal reflux disease and obesity. Gastroenterol Clin North Am. 2010; 39:39–46. [PubMed: 20202577]

Berthoud HR, Patterson LM, Neumann F, Neuhuber WL. Distribution and structure of vagal afferent intraganglionic laminar endings (IGLEs) in the rat gastrointestinal tract. Anat Embryol. 1997; 195:183–191. [PubMed: 9045988]

Beyak MJ. Visceral afferents - determinants and modulation of excitability. Auton Neurosci. 2010; 153:69–78. [PubMed: 19674942]

Beyak, MJ.; Grundy, D. Vagal afferents innervating the gastrointestinal tract. In: Undem, BJ.; Weinreich, D., editors. Advances in vagal afferent neurobiology. Taylor & Francis; Boca Raton: 2005. p. 315-350.

Bielefeldt K, Zhong F, Koerber HR, Davis BM. Phenotypic characterization of gastric sensory neurons in mice. Am J Physiol Gastrointest Liver Physiol. 2006; 291:G987–997. [PubMed: 16728726]

Boeckxstaens GE. The lower oesophageal sphincter. Neurogastroenterol Motil. 2005; 17(Suppl 1):13–21. [PubMed: 15836451]

Brasseur JG, Ulerich R, Dai Q, Patel DK, Soliman AM, Miller LS. Pharmacological dissection of the human gastro-oesophageal segment into three sphincteric components. J Physiol. 2007; 580:961–975. [PubMed: 17289789]

Brierley, SM.; Hughes, P.; Harrington, A.; Blackshaw, LA. Innervation of the gastrointestinal tract by spinal and vagal afferent nerves. In: Johnson, LR.; Ghishan, FK.; Kaunitz, JD.; Merchant, JL.; Said, HM.; Wood, JD., editors. Physiology of the Gastrointestinal Tract, V.1. 5. Elsevier; Amsterdam: 2012. p. 703-731.

Clerc N. Afferent innervation of the lower esophageal sphincter of the cat. Pathways and functional characteristics. J Auton Nerv Syst. 1984; 10:213–216. [PubMed: 6481088]

Clerc N, Condamin M. Selective labeling of vagal sensory nerve fibers in the lower esophageal sphincter with anterogradely transported WGA–HRP. Brain Res. 1987; 424:216–224. [PubMed: 3676824]

Clerc N, Mei N. Vagal mechanoreceptors located in the lower oesophageal sphincter of the cat. J Physiol. 1983; 336:487–498. [PubMed: 6875916]

Falempin M, Mei N, Rousseau JP. Vagal mechanoreceptors of the inferior thoracic oesophagus, the lower oesophageal sphincter and the stomach in the sheep. Pflugers Arch. 1978; 373:25–30. [PubMed: 565031]

Falk GW. Barrett's esophagus. Gastroenterology. 2002; 122:1569–1591. [PubMed: 12016424]

Frisby CL, Mattsson JP, Jensen JM, Lehmann A, Dent J, Blackshaw LA. Inhibition of transient lower esophageal sphincter relaxation and gastroesophageal reflux by metabotropic glutamate receptor ligands. Gastroenterology. 2005; 129:995–1004. [PubMed: 16143137]

Giuli, R.; Galmiche, JP.; Jamieson, GG.; Scarpignato, C. The Esophagogastric Junction. John Libbey Eurotext; Paris: 1998.

Goyal RK, Padmanabhan R, Sang Q. Neural circuits in swallowing and abdominal vagal afferent-mediated lower esophageal sphincter relaxation. Am J Med. 2001; 111(Suppl 8A):95S–105S. [PubMed: 11749933]

Grassi M, Petraccia L, Mennuni G, Fontana M, Scarno A, Sabetta S, Fraioli A. Changes, functional disorders, and diseases in the gastrointestinal tract of elderly. Nutr Hosp. 2011; 26:659–668. [PubMed: 22470008]

Helke, CJ. Vagal afferent neurons: Neurotrophic factors and epigenetic influences. In: Undem, BJ.; Weinreich, D., editors. Advances in vagal afferent neurobiology. Taylor & Francis; Boca Raton: 2005. p. 27-76.

Hershcovici T, Mashimo H, Fass R. The lower esophageal sphincter. Neurogastroenterol Motil. 2011; 23:819–830. [PubMed: 21711416]

Jensen J, Lehmann A, Uvebrant A, Carlsson A, Jerndal G, Nilsson K, Frisby C, Blackshaw LA, Mattsson JP. Transient lower esophageal sphincter relaxations in dogs are inhibited by a metabotropic glutamate receptor 5 antagonist. Eur J Pharmacol. 2005; 519:154–157. [PubMed: 16102747]

Johnson, LR. Physiology of the gastrointestinal tract. 4. Elsevier Academic Press; Burlington, MA: 2006.

Kessing BF, Conchillo JM, Bredenoord AJ, Smout AJ, Masclee AA. Review article: the clinical relevance of transient lower oesophageal sphincter relaxations in gastro-oesophageal reflux disease. Aliment Pharmacol Ther. 2011; 33:650–661. [PubMed: 21219371]

Lehmann A. Novel treatments of GERD: focus on the lower esophageal sphincter. Eur Rev Med Pharmacol Sci. 2008; 12(Suppl 1):103–110. [PubMed: 18924449]

Mazzia C, Clerc N. Ultrastructural relationships of spinal primary afferent fibres with neuronal and non-neuronal cells in the myenteric plexus of the cat oesophagogastric junction. Neuroscience. 1997; 80:925–937. [PubMed: 9276503]

Mazzia C, Clerc N. Ultrastructural analysis of spinal primary afferent fibers within the circular muscle of the cat lower esophageal sphincter. Histochem Cell Biol. 2000; 113:235–239. [PubMed: 10817678]

Mei N, Salducci J, Monges H, Farnarier F. Afferent vagal impulses from the lower oesophageal sphincter of the cat. Rendie Gastroenterol. 1972; 4:65–68.

Mittal, RK. Motor function of the pharynx, the esophagus, and its sphincters. In: Johnson, LR.; Ghishan, FK.; Kaunitz, JD.; Merchant, JL.; Said, HM.; Wood, JD., editors. Physiology of the Gastrointestinal Tract, V.1. 5. Elsevier; Amsterdam: 2012. p. 919-950.

Mittal RK, Holloway RH, Penagini R, Blackshaw LA, Dent J. Transient lower esophageal sphincter relaxation. Gastroenterology. 1995; 109:601–610. [PubMed: 7615211]

Neuhuber WL, Kressel M, Stark A, Berthoud HR. Vagal efferent and afferent innervation of the rat esophagus as demonstrated by anterograde DiI and DiA tracing: focus on myenteric ganglia. J Auton Nerv Syst. 1998; 70:92–102. [PubMed: 9686909]

Neuhuber WL, Raab M, Berthoud HR, Worl J. Innervation of the mammalian esophagus. Adv Anat Embryol Cell Biol. 2006; 185:1–73. [PubMed: 16573241]

Page AJ, Brierley SM, Martin CM, Price MP, Symonds E, Butler R, Wemmie JA, Blackshaw LA. Different contributions of ASIC channels 1a, 2, and 3 in gastrointestinal mechanosensory function. Gut. 2005; 54:1408–1415. [PubMed: 15987792]

Page AJ, Slattery JA, Milte C, Laker R, O'Donnell T, Dorian C, Brierley SM, Blackshaw LA. Ghrelin selectively reduces mechanosensitivity of upper gastrointestinal vagal afferents. Am J Physiol Gastrointest Liver Physiol. 2007; 292:G1376–1384. [PubMed: 17290011]

Phillips RJ, Powley TL. Tension and stretch receptors in gastrointestinal smooth muscle: re-evaluating vagal mechanoreceptor electrophysiology. Brain Res Brain Res Rev. 2000; 34:1–26. [PubMed: 11086184]

Powley TL, Chi MM, Schier LA, Phillips RJ. Obesity: should treatments target visceral afferents? Physiol Behav. 2005; 86:698–708. [PubMed: 16243369]

Powley TL, Gilbert JM, Baronowsky EA, Billingsley CN, Martin FN, Phillips RJ. Vagal sensory innervation of the gastric sling muscle and antral wall: implications for gastro-esophageal reflux disease? Neurogastroenterol Motil. 2012; 24:e526–537. [PubMed: 22925069]

Powley TL, Phillips RJ. Vagal intramuscular array afferents form complexes with interstitial cells of Cajal in gastrointestinal smooth muscle: analogues of muscle spindle organs? Neuroscience. 2011; 186:188–200. [PubMed: 21530617]

Powley TL, Wang XY, Fox EA, Phillips RJ, Liu LW, Huizinga JD. Ultrastructural evidence for communication between intramuscular vagal mechanoreceptors and interstitial cells of Cajal in the rat fundus. Neurogastroenterol Motil. 2008; 20:69–79. [PubMed: 17931338]

Timmermans JP, Adriaensen D. Gastrointestinal mechanosensors: analysis of multiple stimuli may require complex sensors. Neurogastroenterol Motil. 2008; 20:4–7. [PubMed: 18173558]

Vandenplas Y, Hassall E. Mechanisms of gastroesophageal reflux and gastroesophageal reflux disease. J Pediatr Gastroenterol Nutr. 2002; 35:119–136. [PubMed: 12187285]

Wang FB, Powley TL. Topographic inventories of vagal afferents in gastrointestinal muscle. J Comp Neurol. 2000; 421:302–324. [PubMed: 10813789]

Zerbib F. Medical treatment of GORD. Emerging therapeutic targets and concepts. Best Pract Res Clin Gastroenterol. 2010; 24:937–946. [PubMed: 21126705]

Zagorodnyuk VP, Brookes SJ. Transduction sites of vagal mechanoreceptors in the guinea pig esophagus. J Neurosci. 2000; 20:6249–6255. [PubMed: 10934275]

Zagorodnyuk VP, Chen BN, Brookes SJ. Intraganglionic laminar endings are mechano-transduction sites of vagal tension receptors in the guinea-pig stomach. J Physiol. 2001; 534:255–268. [PubMed: 11433006]

Zagorodnyuk VP, Chen BN, Costa M, Brookes SJ. Mechanotransduction by intraganglionic laminar endings of vagal tension receptors in the guinea-pig oesophagus. J Physiol. 2003; 553:575–587. [PubMed: 14500769]

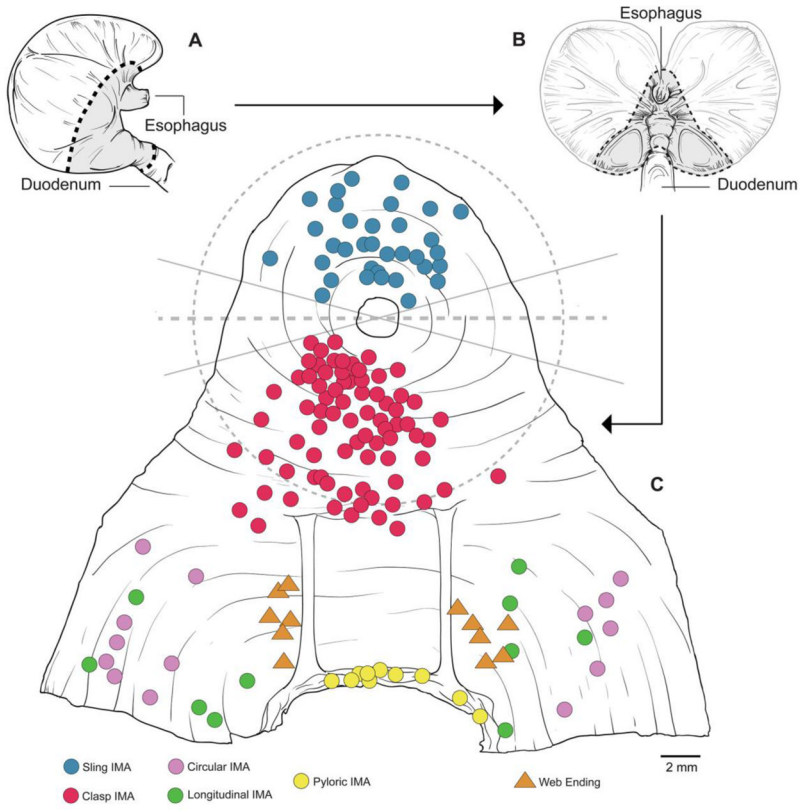

Figure 1.

The preparation of the LES-antral whole mounts that were examined for the inventory of endings and a map of the intramuscular arrays (IMAs) digitized and traced with Neurolucida. **A**. A dorsal side of the stomach illustrating the cut lines used (dashed lines) and the esophageal, LES, antral and pyloric tissue included in the whole mount (gray region). **B**. A mucosa-side view of the stomach, opened on the greater curvature, illustrating the cut lines and whole mount region designated as in panel A. **C**. A schematic of a normalized whole mount prepared, serosa up, once the mucosa and submucosa had been removed and the tissue had been processed with DAB, cleared, and flattened on a slide (the incision to remove the cupping of the cardia is not shown). The individual IMAs evaluated quantitatively are indicated with symbols. Once spread and flattened, the region of the whole mount concentric to the esophagus and containing clasp and sling muscle fibers had a radius of roughly 9 mm, as designated with the dashed circular line. The two solid lines that intersect at the middle of the lumen of the esophagus delimit the region of ±15° of a "frontal" equator (represented by the horizontal dashed line) where (a) clasp and sling muscles intermingled and IMAs could not be unequivocally classified as clasp or sling endings and (b) the terminals were compromised by the tissue incision employed to flatten the specimen. The locations of the sling IMAs analyzed are indicated with blue symbols; the locations of the clasp IMAs analyzed are indicated with red symbols. The red-colored IMA symbols that fall outside the circular clasp-sling measurement region designated by the dashed circle were probable LES endings outside the sampled region (but not included in the sample quantified). Also indicated are antral endings (purple and green) and pyloric endings (yellow) that were examined for comparisons with the clasp and sling IMAs. Additionally, the locations of the antral web ending afferents (gold triangles) used for comparative purposes are also designated.

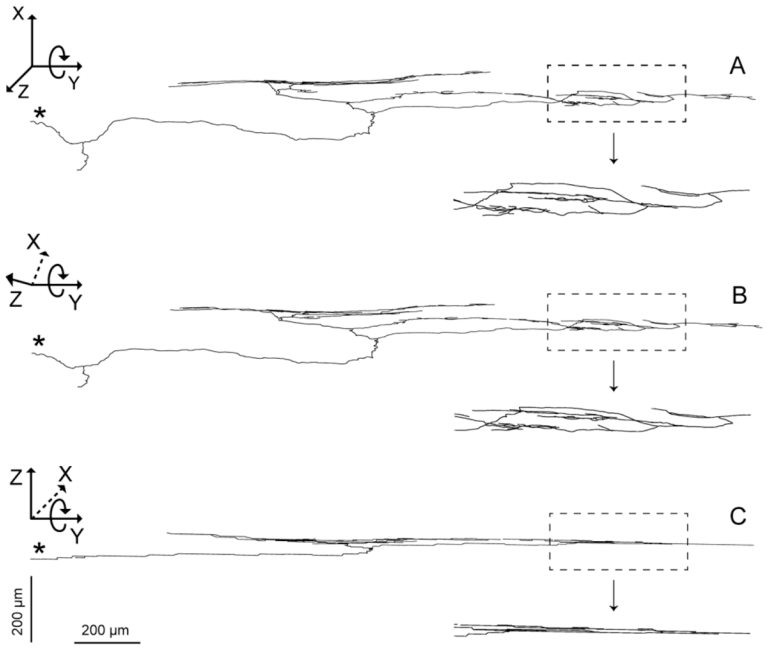

Figure 2.

A tracing of an IMA from the LES in the digital coordinate space of the Neurolucida software. The morphometry software renders afferent arbors as 3D stick figures with multiple features quantified (for photomicrographic 2D renderings of IMAs, see Figs. 3 and 4). **Panel A**: A parent neurite (designated with an asterisk) enters at 9:00 o'clock, travels to the middle of the panel, and then bifurcates repeatedly to form the IMA arbor. The window on right shows at a higher power the pattern of branching in the arbor. The dimensions of the full IMA arbor can be gauged using the scale bars at the bottom of Panel C. **Panels B and C** illustrate that, in the software coordinate space, arbors can be rotated and measured from any perspective. In the examples illustrated, the Z-axis of the IMA is rolled 45° around the Y-axis (in panel B) and then another 45° around the Y-axis (in panel C) to examine the planar arbor in side view or at 90° to the perspective in Panel A. The scale bars apply to main section of each of the three panels: the horizontal scale applies to the Y-dimension, and the vertical scale applies to both the X- and Z-dimensions.

Figure 3.

A representative dextran-biotin labeled clasp muscle IMA. In the center, a Photoshop tracing of the IMA terminal arbor illustrates an incoming parent fiber (at about 8:00 o'clock) that bifurcates and branches repeatedly to produce a typical array of long terminal processes that run in and parallel to clasp muscle fibers (not stained). Panels **A through D** are high-power all-in-focus photomicrographs of neurites from the traced IMA taken at the locations in the tracing designated by the corresponding letters. The tracing scale bar = 250 μm; the scale bar in Panel C = 20 μm for all four photomicrographs.

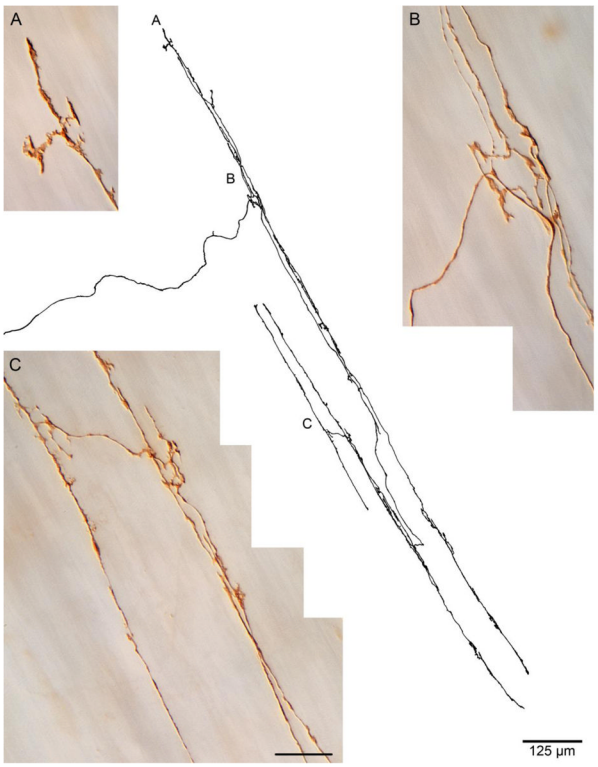

Figure 4.

A representative dextran-biotin labeled sling muscle IMA. In the center, a Photoshop tracing of the IMA terminal arbor illustrates the incoming parent fiber that bifurcates and branches repeatedly to produce a terminal field of long processes that run in and parallel to sling muscle fibers (not stained). Panels **A through C** are high power all-in-focus photomicrographs of neurites in the terminal of the traced ending, taken at the locations in the tracing designated by the corresponding letters. The tracing scale bar = 125 μm; the scale bar in Panel C = 20 μm for all three photomicrographs.

Figure 5.

A sample of representative sling and clasp IMAs traced with Photoshop. All IMA terminals are reproduced at the same scale (bottom of figure). As noted in the quantitative analysis of sling and clasp endings mapped on the schematic in Figure 1C, IMAs innervating clasp fibers, although qualitatively very similar in structure, were statistically larger and had more numerous branches than sling IMAs. The tracing scale bar = 250 μm.

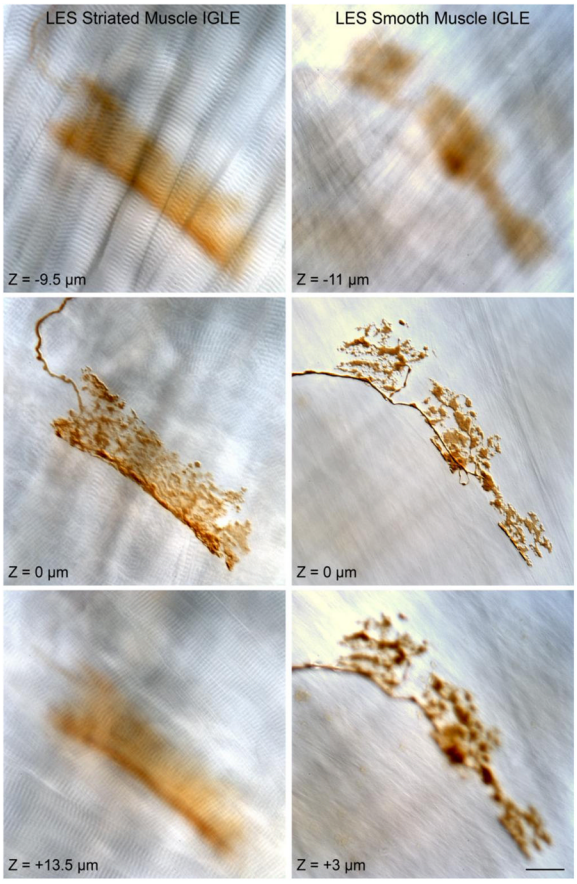

Figure 6.

Representative intraganglionic laminar endings (IGLEs) that were observed in the myenteric plexus (not stained) between muscle sheets of both striated muscle (illustrated in the left column) and smooth muscle (illustrated in the right column) sheets in the LES area. Each of the two columns of micrographs show single-plane images taken from a z-stack of DIC images with the IGLE in-focus in the middle row of the stack (and designated as Z = 0 µm for the respective middle micrographs in each column). For the IGLE associated with striated muscle (left column), the DIC micrographs from below and above the focal plane of the IGLE illustrate the signature A and I bands of striated muscle. For the IGLE associated with smooth muscle (right column), the DIC images from below and above the focal plane of the IGLE illustrate the characteristic smooth muscle patterns. The scale bar in the lower right hand image = 20 µm for all micrographs.

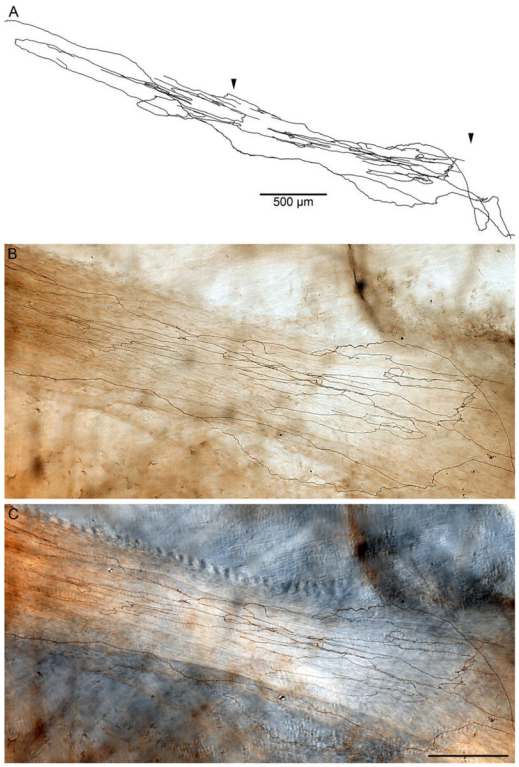

Figure 7.

A segment of an elongated IMA innervating a principle sling muscle bundle (the full length of the bilateral principle bundles are illustrated in the whole mount schematic in Figure 1C) that runs between the smooth muscle ring that forms the LES and the distal antropyloric area where the bundle attaches to the antral muscle sheets. **A**. is a Photoshop tracing through a portion of the IMA. The two arrowheads designate the portion of the IMA segment in Panels B and C. Panel **B** is a low power brightfield photomicrograph of a field that illustrates the DAB stained neurites of the IMA, whereas Panel **C** is a corresponding low power DIC photomicrograph of same field that illustrates more clearly the unstained principle bundle (which runs from left to right) in which the IMA is distributed. The tracing scale bare in A = 500 μm; the scale bar in Panel C = 250 μm for panels B,C.

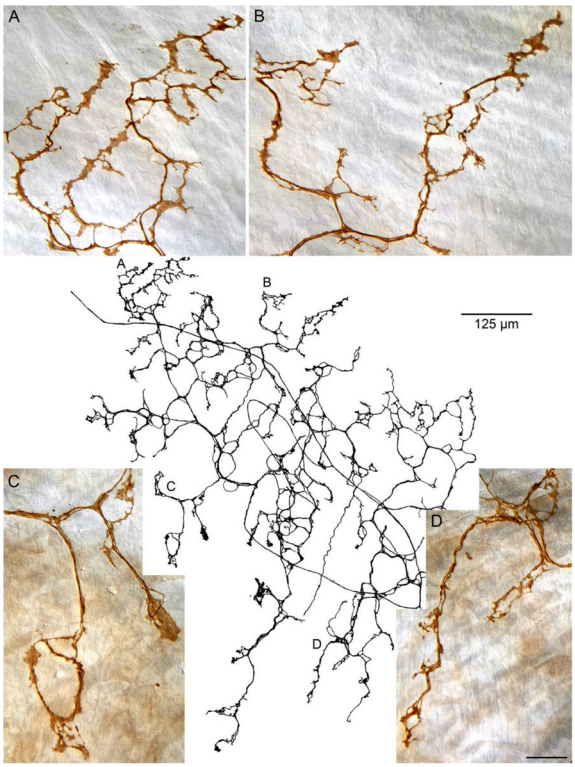

Figure 8.

The primary plate of subserosal terminals of a web ending, the vagal afferent ending that innervates the distal antral site where the principle sling bundle attaches to the antral muscle sheets (cf. Fig. 1C). In the center of the figure, a Photoshop tracing illustrates a vagal afferent fiber entering the field (at ~ 10:30), traversing the area diagonally, and looping back to arborize as an antral web. Panels **A through D** are all-in-focus photomicrographs taken at the sites in the tracing with the corresponding letters that illustrate the characteristic lamellar and loop patterns of termination of the web processes. The tracing scale bar = 125 μm; the scale bar in Panel D = 20 μm and applies to all four photomicrographs.